1

Humanoid Robot Navigation Based on Groping Locomotion Algorithm to Avoid an Obstacle

Hanafiah Yussof[1], Mitsuhiro Yamano[2], Yasuo Nasu[2], Masahiro Ohka[1]
[1]*Graduate School of Information Science, Nagoya University*
[2]*Faculty of Engineering, Yamagata University*
Japan

1. Introduction

A humanoid robot is a robot with an overall appearance based on that of the human body (Hirai et al., 1998, Hirukawa et al., 2004). Humanoid robots are created to imitate some of the same physical and mental tasks that humans undergo daily. They are suitable to coexist with human in built-for-human environment because of their anthropomorphism, human friendly design and applicability of locomotion (Kaneko et al., 2002). The goal is that one day humanoid robots will be able to both understand human intelligence and reason and act like humans. If humanoids are able to do so, they could eventually coexist and work alongside humans and could act as proxies for humans to do dangerous or dirty work that would not be done by humans if there is a choice, hence providing humans with more safety, freedom and time.

Bearing in mind that such robots will be increasingly more engaged in human's environment, it is expected that the problem of "working coexistence" of humans and humanoid robots will become acute in the near future. However, the fact that no significant rearrangment of the human's environment to accomodate the presence of humanoids can be expected. Eventually, the "working coexistence" of humans and robots sharing common workspaces will impose on robots with their mechanical-control structure at least two classes of tasks: motion in a specific environment with obstacles, and manipulating various objects from the human's environment (Vukobratovic et al., 2005). As far as this working coexistence is concerned, a suitable navigation system combining design, sensing elements, planning and control embedded in a single integrated system is necessary so that humanoid robots can further "adapt" to the environment previously dedicated only to humans. To date, research on humanoid robots has arrived at a point where the construction and stabilization of this type of robot seems to be no longer the key issue. At this stage, it is novel practical applications such as autonomous robot navigation (Saera & Schmidt, 2004, Tu & Baltes, 2006), telerobotics (Sian et al., 2002) and development of intelligent sensor devices (Omata et al., 2004) that are being studied and attracting great interest. Autonomous navigation of walking robots requires that three main tasks be solved: self-localization, obstacle avoidance, and object handling (Clerentin et al., 2005). In current research, we proposed a basic contact interaction-based navigation system called "groping locomotion" on the humanoid robots capable of defining self-localization and obstacle avoidance. This system is based on contact interaction with the aim of creating suitable algorithms for

Source: Mobile Robots Towards New Applications, ISBN 3-86611-314-5, Edited by Aleksandar Lazinica, pp. 784, ARS/plV, Germany, December 2006

humanoid robots to effectively operate in real environments. In order to make humanoid robot recognize its surrounding, six-axis force sensors were attached at both robotic arms as end effectors for force control.

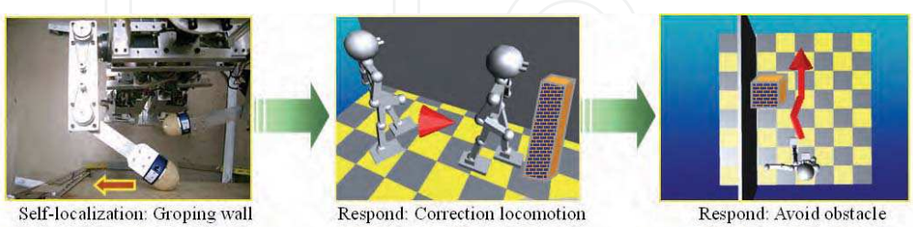

Fig. 1. Robot locomotion in the proposed autonomous navigation system.

Figure 1 explains the phylosophy of groping locomotion method on bipedal humanoid robot to satisfy tasks in autonomous navigation. Referring to this figure, the humanoid robot perform self-localization by groping a wall surface, then respond by correcting its orientation and locomotion direction. During groping locomotion, however, the existence of obstacles along the correction area creates the possibility of collisions. Therefore, the humanoid robot recognize the existance of obstacle in the correction area and perform obstacle avoidance to avoid the obstacle.

Some studies on robotics have led to the proposal of an obstacle avoidance method employing non-contact interaction, such as vision navigation and image processing (Seydou et al., 2002, Saera & Schmidt, 2004), while others use armed mobile robots and humanoids on a static platform (Borenstein & Koren, 1991). There has been very little research reported about the application of a contact interaction method to avoid obstacles in anthropomorphic biped humanoid robots. In this report, we focus on a development of an autonomous system to avoid obstacles in groping locomotion by applying multi-tasking algorithm on a bipedal 21-DOF (degrees-of-freedom) humanoid robot *Bonten-Maru II*. Consiquently, we presents previously developed bipedal humanoid robot *Bonten-Maru II* that used in the experiments and evaluations of this research project. In addition, we explain the overall structure of groping locomotion method and its contribution in the humanoid robot's navigation system. We also explain simplified formulations to define trajectory generation for 3-DOF arms and 6-DOF legs of *Bonten-Maru II.* Furthermore, this report includes an experimental results of the proposed obstacle avoidance method using *Bonten-Maru II* that were conducted in conjunction with the groping locomotion experiments.

2. Relevancy of Contact Interaction in Humanoid Robot's Navigation

Application of humanoid robots in the same workspace with humans inevitably results in contact interaction. Our survey on journals and technical papers resulted to very small number of work reported about the application of a contact interaction method to navigate humanoid robots in real environments. Some studies in robotics have proposed methods of interaction with environments using non-contact interaction such as using ultrasonic wave sensor, vision image processing and etc (Ogata et al., 2000, Cheng et al., 2001). However, some work reported the use of robotic armed mobile robot to analyze object surface by groping and obtain information to perform certain locomotion (Hashimoto et al., 1997, Kanda at al., 2002, Osswald et al., 2004). Overall there has been very little work reported

about application of contact interaction on bipedal humanoid robots (Konno, 1999). Eventually, most report in navigation of walking robot is related to perception-guided navigation (Clerentin et al., 2005), particularly related to visual-based navigation that has been a relevant topic for decades. In visual-based navigation, which is classified as non-contact interaction, besides the rapid growth in visual sensor technology and image processing technology, identification accuracy problems due to approximate data obtained by the visual sensor and interruption of environment factors such as darkness, smoke, dust, etc. seems to reduce the robots performances in real environments.
Meanwhile, contact interaction offers better options for humanoid robots to accurately recognize and structure their environment (Coelho et al., 2001, Kim et al., 2004), making it easier for them to perform tasks and improve efficiency to operate in real environment. We believe that contact interaction is a relevant topic in research and development of humanoid robot's navigation. Indeed contact interaction is a fundamental feature of any physical manipulation system and the philosophy to establish working coexistence between human and robot.

3. Definition of Groping Locomotion

Groping is a process in which the humanoid robot keeps its arm in contact with the wall's surface while performing a rubbing-like motion. The proposed groping locomotion method comprises a basic contact interaction method for the humanoid robot to recognize its surroundings and define self-localization by touching and groping a wall's surface to obtain wall orientation (Hanafiah et al., 2005a, Hanafiah et al., 2005b). Figure 2 shows photograph of the robot and robot's arm during groping on the wall surface. During groping process, position data of the end effector are defined, which described the wall's surface orientation. Based on the wall's orientation, relative relations of distance and angle between the robot and the wall are obtained. The robot then responds to its surroundings by performing corrections to its orientation and locomotion direction. Basically, the application of sensors is necessary for a humanoid robot to recognize its surroundings. In this research, six-axis force sensors were attached to both arms as end effectors that directly touch and grasp objects and provide force data that are subsequently converted to position data by the robot's control system.

Fig. 2. Photographs of robot and robot's arm during groping on wall surface.

In this research, the groping process is classified into two situations: groping the front wall and groping the right-side wall. Figures 3(a) and (b) shows plotted data of the end effector position during groping front wall and right-side wall, which described the wall surface orientation that positioned at the robot's front and right side, respectively. The end effector data obtained during groping process are calculated with the least-square method to define wall's orientation. Based on the wall's orientation obtained in groping process, the relative relation of humanoid robot's

position and angle are defined, like shown in Fig. 4. Here, ϕ is groping angle , and $90° - \phi$ is a correction angle. Meanwhile L is the shortest distance from the humanoid robot to the wall.

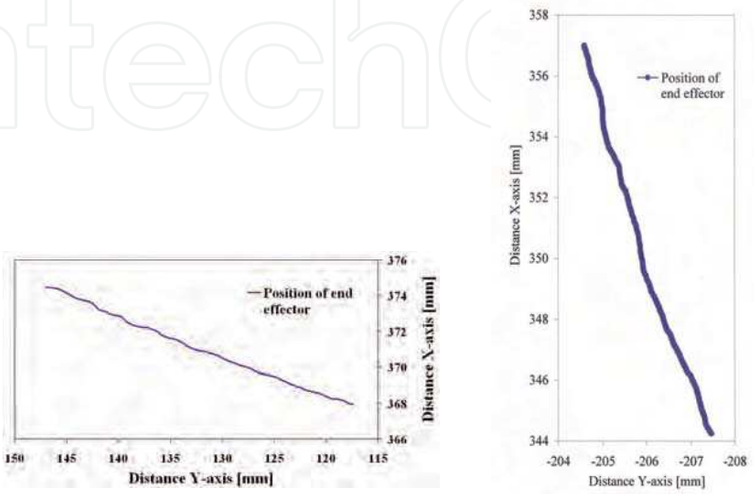

(a) Groping front (b) Groping right-side

Fig. 3. Graph of end effector position in groping locomotion.

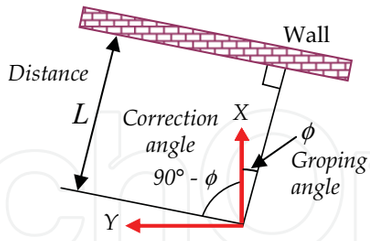

Fig. 4. Robot orientation after groping wall.

4. Obstacle Avoidance in Groping Locomotion Method

4.1 Definision of Obstacle Avoidance in Humanoid Robot Navigation System

In humanoid robot navigation, abilities to recognize and avoid obstacles are inevitably important tasks. The obstacle avoidance method proposed in this research is a means to recognize and avoid obstacles that exist within the correction area of groping locomotion by

applying a suitable algorithm to the humanoid robot's control system. The proposed obstacle avoidance algorithm is applied to a bipedal humanoid robot whose arms were equipped with six-axis force sensors functioned to recognize physically the presence of obstacles, then ganerate suitable trajectory to avoid it.

4.2 Groping Locomotion Algorithm

In the groping-locomotion method, an algorithm in the humanoid robot's control system controls the motions of the robot's arms and legs based on information obtained from groping process. The algorithm comprises kinematics formulations to generate trajectory for each robotic joint. The formulations involve solutions to forward and inverse kinematics problems, and interpolation of the manipulator's end effector. It also consists of force-position control formulations to define self-localizasion of the humanoids body based on force data that obtained in groping process. Figure 5 shows a flowchart of the groping locomotion algorithm. Basically, the algorithm consists of three important processes: searching for a wall, groping a wall's surface, and correction of robot position and orientation. The algorithm is applied within the humanoid robot control system. Figure 6 displays the control system structure consists of two main process to control the humanoid robot motion: robot controller and motion instructor. Shared memory is used for connection between the two processes to send and receive commands. The motion instructor, also known as user controller, initially check whether instruction from robot controller has an access permission or not before motion instructor sending request motion commands to perform motion. The command requested by motion instructer is send to shared memory and transfer to robot controller. Based on groping locomotion algorithm, the robot controller generate nacessary trajectory and send its commands to humanoid robot's joints in order to perform required motion. Lastly, when the motion is completed, new access permission will send to motion instructor for delivery of the next instruction commands.

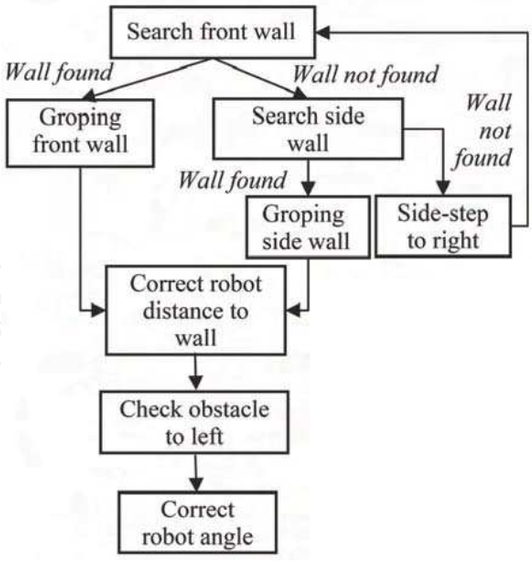

Fig. 5. Groping locomotion algorithm.

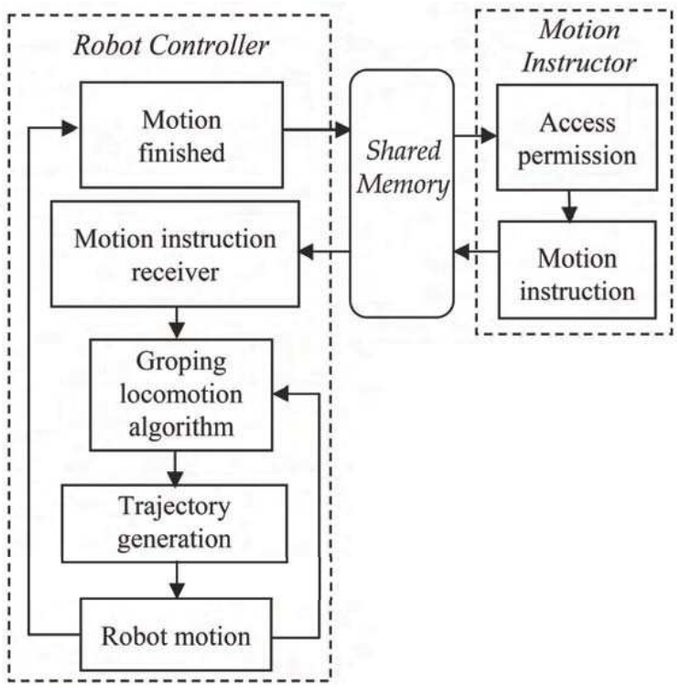

Fig. 6. Control system structure of humanoid robot *Bonten-Maru II*.

4.3 Correlation of Obstacle Avoidance with Groping Locomotion Algorithm

Research on groping locomotion has led to the proposal of a basic contact interaction method in humanoid robot's navigation system. In groping locomotion, a robot's arm gropes a wall surface to obtain the wall's orientation data by keeping its arm in contact with the wall's surface, and corrects its position and orientation to become parallel with the wall. Here, the proposed obstacle avoidance method is designed to avoid obstacles existing at the correction area. Figure 7(a) shows flowchart of the obstacle avoidance algorithm. The algorithm consists of three important processes: checking the obstacle to the left, rotating toward the back-left position, and confirming the obstacle's presence. The algorithm is based on trajectory generation of the humanoid robot's legs, with reference to the groping results in groping locomotion. Meanwhile, Fig. 7(b) shows the flowchart of groping locomotion algorithm combined with the proposed obstacle avoidance algorithm. The combined algorithm is complied in the robot's control system, as described in Fig. 6, to perform tasks in humanoid robot's navigation system.

4.4 Analysis of Obstacle Avoidance Algorithm

The concept of the proposed obstacle-avoidance algorithm is based on trajectory generation of the humanoid robot's legs, with reference to the groping results. Leg positions are decided by interpolation using polynomial equations, and each leg-joint position is given via angle data from calculation of the inverse kinematics needed to move the legs to the desired positions.

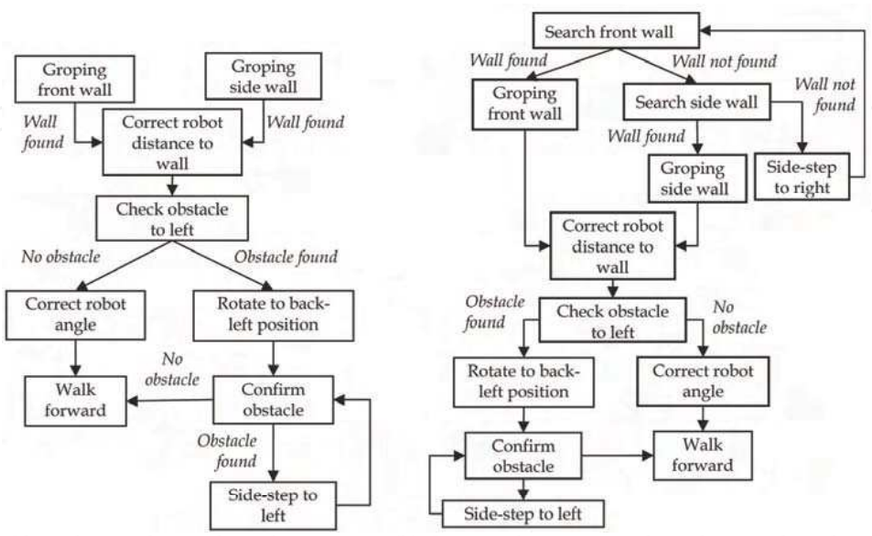

(a) Obstacle avoidance algorithm. (b) Groping locomotion algorithm combined with obstacle avoidance algorithm.

Fig. 7. Application of obstacle avoidance algorithm to groping locomotion algorithm.

Basically, obstacle avoidance is performed after correcting the robot's distance to the wall, before proceeding to the correct angle. While checking the obstacle to the left, the left arm will search for and detect any obstacle that exists within the correction angle's area and up to the arm's maximum length in order to instruct the robot's system either to proceed with the correction or to proceed with the next process of obstacle avoidance. If an obstacle is detected, the robot will rotate to the back-left position, changing its orientation to face the obstacle. The robot will then continuously recheck the existence of the obstacle by performing the "confirm obstacle" process. If no obstacle is detected, the robot will walk forward. However, if an obstacle was detected, instead of walking to forward direction, the robot will walk side-step towards its left side direction, and repeat again the confirmation process until no obstacle is detected. The robot will then walks forward and complete the obstacle avoidance process.

4.4.1 Checking for Obstacles to the Left

While checking for an obstacle, if the arm's end effector touches an object, the force sensor will detect the force and send the force data to the robot's control system. Once the detected force exceeds the parameter value of maximum force, motion will stop. At this moment, each encoder at the arm's joints will record angle data and send them to the robot control system. By solving the direct kinematics calculation of the joint angles, the end effector's position is obtained. The left arm's range of motion while checking for obstacles is equal to the correction angle, $90° - \phi$, where ϕ is the groping angle. Any objects detected within this range are considered as obstacles.

4.4.2 Rotate to Back-Left Position

Once an obstacle has been detected during the process of checking for an obstacle to the left, the robot will rotate its orientation to the back-left position "facing" the obstacle in order to

confirm the obstacle's position at a wider, more favorable angle, finally avoiding it. At first, the left leg's hip-joint yaw will rotate counterclockwise direction to $90° - \phi$. At the same time, the left leg performs an ellipse trajectory at *Z*-axis direction to move the leg one step backward to a position defined at *X*-*Y* axes plane. At this moment the right leg acts as the support axis. The left leg's position is defined by interpolation of the leg's end point from its initial position with respect to the negative *X*-axis position and positive *Y*-axis position of the reference coordinate at a certain calculated distance. Then, the robot corrects its orientation by changing the support axis to the left leg and reverses the rotation clockwise of the left leg's hip-joint yaw direction of the angle $90° - \phi$. Finally, the robot's orientation is corrected to "face" the obstacle.

4.4.3 Confirm Obstacle

After the obstacle is detected and the robot orientation has changed to face the obstacle, it is necessary to confirm whether the obstacle still exists within the locomotion area. This process is performed by the robot's right arm, which searches for any obstacle in front of the robot within its reach. If the obstacle is detected within the search area, the arm will stop moving, and the robot will perform side-step to left direction. The robot's right arm will repeat the process of confirming the obstacle's presence until the obstacle is no longer detected. Once this happens, the robot will walk forward in a straight trajectory. These steps complete the process of avoiding the obstacle.

5. Application of Groping Locomotion Method in Humanoid Robot Navigation System

The development of navigation system for humanoid robots so that they can coexist and interact with humans and their surroundings, and are able to make decisions based on their own judgments, will be a crucial part of making them a commercial success. In this research, we proposed a basic navigation system called "groping locomotion" on a 21-DOF humanoid robot *Bonten-Maru II*. The groping locomotion method consists of algorithms to define self-localization and obstacle avoidance for bipedal humanoid robot. This system is based on contact interaction with the aim of creating suitable algorithms for humanoid robots to effectively operate in real environments.

5.1 Humanoid Robot *Bonten-Maru II*

In this research, we have previously developed a 21-DOF (degrees-of-freedom), 1.25-m tall, 32.5-kg anthropomorphic prototype humanoid robot called *Bonten-Maru II*. The *Bonten-Maru II* was designed to mimic human characteristics as closely as possible, especially in relation to basic physical structure through the design and configuration of joints and links. The robot has a total of 21 DOFs: six for each leg, three for each arm, one for the waist, and two for the head. The high numbers of DOFs provide the *Bonten-Maru II* with the possibility of realizing complex motions. Figure 8 shows a photograph of *Bonten-Maru II*, the configuration of its DOFs, and physical structure design.

The configuration of joints in *Bonten-Maru II* that closely resemble those of humans provides the advantages for the humanoid robot to attain human-like motion. Each joint features a relatively wide range of rotation angles, shown in Table 1, particularly for the hip yaw of both legs, which permits the legs to rotate through wide angles when avoiding obstacles. Each joint is driven by a DC servomotor with a rotary encoder and a harmonic drive-

reduction system, and is controlled by a PC with the Linux OS. The motor driver, PC, and power supply are placed outside the robot.

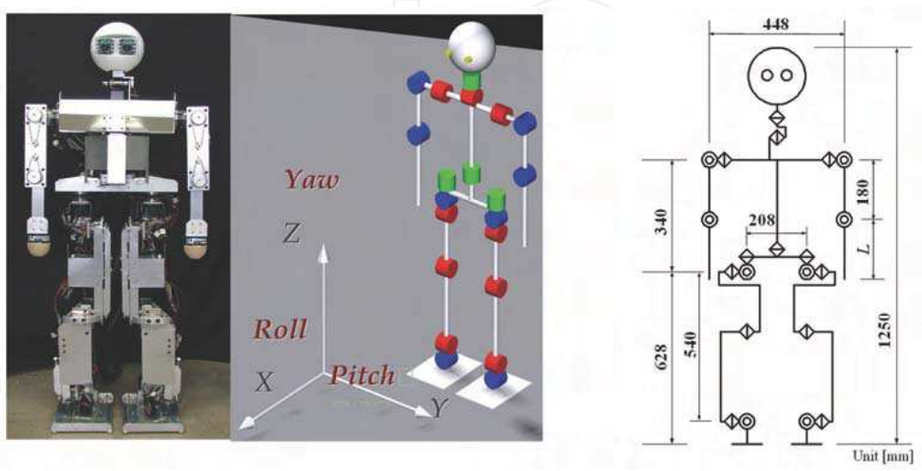

Fig. 8. Humanoid robot *Bonten-Maru II* and configuration of DOFs and joints.

Axis	*Bonten-Maru II* (deg)
Neck (roll and pitch)	-90 ~ 90
Shoulder (pitch) right & left	-180 ~ 120
Shoulder (roll) right/left	-135 ~ 30/-30 ~ 135
Elbow (roll) right/left	0 ~ 135/0 ~ -135
Waist (yaw)	-90 ~ 90
Hip (yaw) right/left	-90 ~ 60/-60 ~ 90
Hip (roll) right/left	-90 ~ 22/-22 ~ 90
Hip (pitch) right & left	-130 ~ 45
Knee (pitch) right & left	-20 ~150
Ankle (pitch) right & left	-90 ~ 60
Ankle (roll) right/left	-20 ~ 90/-90 ~ 20

Table 1. Joint rotation angle.

In current research, *Bonten-Maru II* is equipped with a six-axis force sensor in both arms. As for the legs, there are four pressure sensors under each foot: two under the toe area and two under the heel. These provide a good indication that both legs are in contact with the ground. The *Bonten-Maru II*'s structure design and control system are used in experiments and evaluations of this research.

5.2. Self-Localization: Defining Humanoid Robot's Orientation from Groping Result

The end effector data obtained during groping process are calculated with the least-square method to result a linear equation as shown in Eq. (1). Here, distance and groping angle between the robot to the wall, described as L and ϕ, respectively, are defined by applying formulations shown at belows. At first, a straight line from the reference coordinates origin and perpendicular with Eq. (1), which described the shortest distance from robot to wall, is defined in Eq. (2), where the intersection coordinate in X-Y axes plane is shown in Eq. (3).

$$y=ax+b \tag{1}$$

$$y=-\frac{1}{a}x \tag{2}$$

$$\begin{bmatrix} C_x \\ C_y \end{bmatrix} = \begin{bmatrix} -\dfrac{ab}{a^2+1} \\ \dfrac{b}{a^2+1} \end{bmatrix} \tag{3}$$

Groping angle ϕ is an angle from *X*-axis of the robot reference coordinates to the perpendicular line of Eq. (2). Here, distance *L* and groping angle ϕ are shown in Eqs. (4) and (5), respectively (also refer Fig. 4). In this research, correction of the robot position and orientation are refers to values of *L* and ϕ. Eventually, correction of the robot's locomotion direction basically can be defined by rotating the robot's orientation to angle 90°-ϕ, so that robot's orientation becomes parallel with the wall's orientation.

$$L=\frac{b}{\sqrt{a^2+1}} \tag{4}$$

$$\phi=\tan^{-1}\left(-\frac{1}{a}\right) \tag{5}$$

5.3 Correction of Humanoid Robot's Orientation and Locomotion Direction

5.3.1 Correction of distance

Figure 9 shows top view of structural dimensions of *Bonten-Maru II* and groping area of the robot's arm. This figure is used to explain formulations to define correction of diatance for groping front wall and right-side

Groping front wall

In groping front wall, position of the wall facing the robot creates possibility of collision during correction of the robot's orientation. Therefore, correction of robot's distance was simply performed by generating trajectory for legs to walk to backwards direction. Here, quantity of steps are required to define. The steps quantity are depends on distance of the robot to the wall, and calculations considering the arm's structural dimension and step size (length of one step) for the utilized humanoid robot's leg. The formulation to define quantity of steps is shown in following equation.

$$q=\begin{cases} n & (L_1 < L \le L_m) \\ n-1 & (L_m < L \le L_t) \end{cases} \tag{6}$$

Here, *q* is step quantity, and *L* is the measured distance (shortest distance) from the intersection point of right arm's shoulder joints to the wall, which obtained from groping result. Refer to Fig. 9, during process of searching for wall, only elbow joint is rotating while the two shoulder joints are remain in static condition. Here, L_1 is dimension from the

shoulder joints to the elbow joint, L_t is the total length of arm from the shoulder joints to the end effector, and L_3 is the step size of the robot's leg. Consequently, L_m that indicate in Eq.6 is defined from following equation:

$$L_m = \frac{L_1 + L_3}{2} + L_1 \tag{7}$$

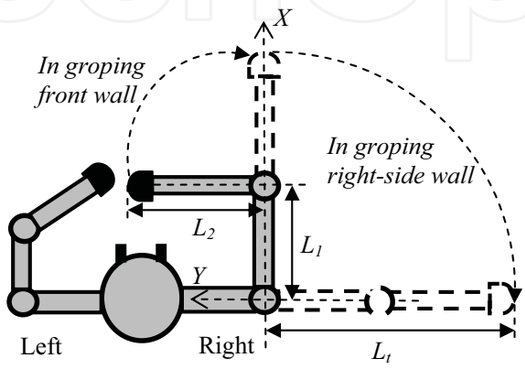

Fig. 9. Structural dimensions and groping area of the humanoid robot's arm.

Groping right-side wall

In groping right-side wall, correction of distance involves trajectory generation of legs to walk side-step away from the wall. However, if the groping angle ϕ is $0<\phi\leq45°$, it is still possible for the robot to collide with the wall. In this case, the robot will walk one step to backward direction, before proceed to walk side-step. Eventually, if the groping angle ϕ is $45°<\phi\leq90°$, the robot will continue to correct its position by walking side-step away from the wall. At this moment, the side-step size S is defined from Eq. (8). Here, L is the distance between the robot to the wall, while L_b is a parameter value which considered safety distance between the robot to the wall during walking locomotion. Parameter value of L_b is specified by the operator which depends on the utilized humanoid robots.

$$S = (L_b - L)\sin\phi \tag{8}$$

Continuously, from Eq. (8), boundary conditions are fixed as following Eqs. (9) and (10). Here, a and β are parameter values which consider maximum side-step size of the humanoid robot legs. Value of a is fixed at minimum side-step size, while β is fixed at maximum side-step size.

$$S = \begin{cases} \alpha & (L_b - L \leq 0) \\ (L_b - L)\sin\phi & (L_b - L > 0) \end{cases} \tag{9}$$

$$S = \begin{cases} \beta & ((L_b - L)\sin\phi > \beta) \\ (L_b - L)\sin\phi & ((L_b - L)\sin\phi \leq \beta) \end{cases} \tag{10}$$

5.3.2 Correction of angle

Correction of the robot's angles is performed by changing the robot orientation to $90°-\phi$, so that the final robot's orientation is parallel with wall's surface orientation. Figure 10 (a) ~ (c) shows a sequential geometrical analysis of the robot's foot-bottom position during correction of angle. From this figure, *X*-*Y* axes is a reference coordinates before rotation, while *X'*-*Y'* axes is the new reference coordinate after the rotation. Here, a is distance from foot center position to the robot's body center position, while b is correction value to prevent flexure problem at the robot's legs. Position of the left foot bottom to correct robot's angle in *X*-*Y* axes plane are described as ψ and δ, as shown in Fig. 10 (b). In this research, value of ψ is fixed to be half of the humanoid robot's step size, while value of δ is defined from following equation.

$$\delta = 2a + b + \psi \tag{11}$$

Figures 11(a) and (b) are respectively shows geometrical analysis of the robot's position and orientation at *X*-*Y* axes plane before and after correction of distance and angle in groping front wall and groping right-side wall, based on groping result. Axes *X*-*Y* indicating orientation before correction, while axes *X'*-*Y'* are after correction is finished.

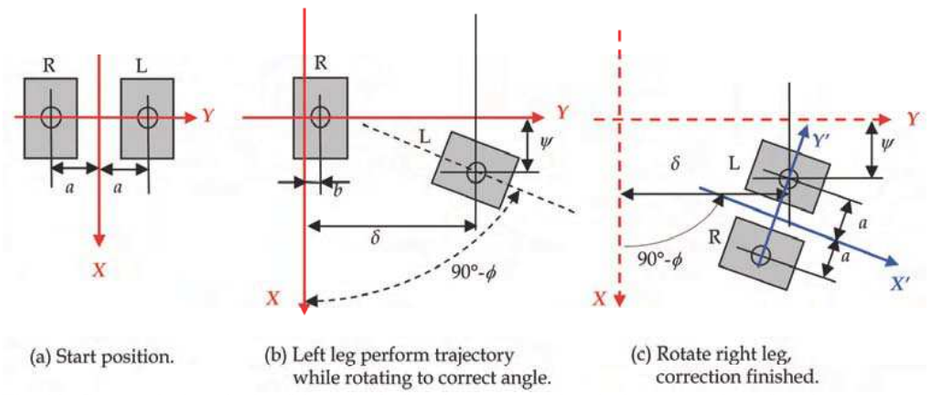

Fig. 10. Geometrical analysis of the robot's foot-bottom position during correction of angle.

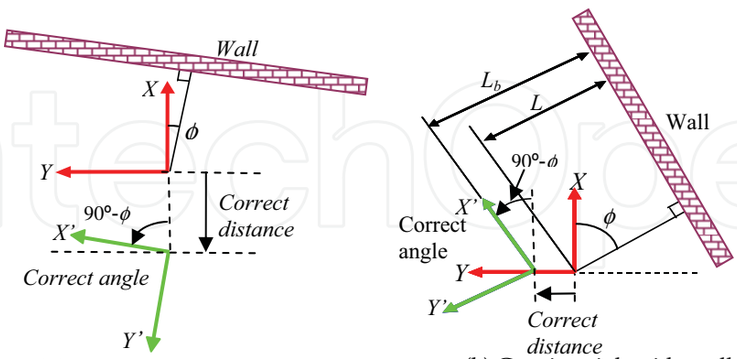

Fig. 11. Geometrical analysis of humanoid robot's orientation in groping front wall and right-side wall.

6. Trajectory Generation in Groping Locomotion to Avoid Obstacle

The formulation and optimization of joint trajectories for a humanoid robot's manipulator is quite different from standard robots' because of the complexity of its kinematics and dynamics. This section presents a formulation to solve kinematics problems to generate trajectory for a 21-DOF humanoid robot in the obstacle avoidance method. The detail kinematics formulations are applied within the algorithm of the groping-locomotion method.

Robot kinematics deals with the analytical study of the geometry of a robot's motion with respect to a fixed reference coordinate system as a function of time without regarding the force/moments that cause the motion. Commonly, trajectory generation for biped locomotion robots is defined by solving forward and inverse kinematics problems (Kajita et al., 2005). In a forward kinematics problem, where the joint variable is given, it is easy to determine the end effector's position and orientation. An inverse kinematics problem, however, in which each joint variable is determined by using end-effector position and orientation data, does not guarantee a closed-form solution. Traditionally three methods are used to solve an inverse kinematics problem: geometric, iterative, and algebraic (Koker, 2005). However, the more complex the manipulator's joint structure, the more complicated and time-consuming these methods become. In this paper, we propose and implement a simplified approach to solving inverse kinematics problems by classifying the robot's joints into several groups of joint coordinate frames at the robot's manipulator. To describe translation and rotational relationship between adjacent joint links, we employ a matrix method proposed by Denavit-Hartenberg (Denavit & Hartenberg, 1995), which systematically establishes a coordinate system for each link of an articulated chain (Hanafiah et al., 2005c).

6.1 Kinematics analysis of a 3-DOF humanoid robot's arm

The humanoid robot *Bonten-Maru II* has three DOFs on each arm: two DOFs (pitch and roll) at the shoulder joint and one DOF (roll) at the elbow joint. Figure 12 shows the arm structure and distribution of joints and links. This figure also displays a model of the robot arm describing the distributions and orientation of each joint coordinates. The coordinate orientation follows the right-hand law, and a reference coordinate is fixed at the intersection point of two joints at the shoulder. To avoid confusion, only the X and Z axes appear in the figure. The arm's structure is divided into five sets of joint-coordinates frames as listed below:

$\sum_0$: Reference coordinate.
$\sum_1$: Shoulder joint pitch coordinate.
$\sum_2$: Shoulder joint roll coordinate.
$\sum_3$: Elbow joint roll coordinate.
$\sum_h$: End-effector coordinate.

Consequently, corresponding link parameters of the arm can be defined as shown in Table 2. From the Denavit-Hartenberg convention mentioned above, definitions of the homogeneous transform matrix of the link parameters can be described as follows:

$$ {}^{0}_{h}T = \mathbf{Rot}(z, \theta)\mathbf{Trans}(0,0,d)\mathbf{Trans}(a,0,0)\mathbf{Rot}(x, \alpha) \tag{12} $$

Link	$\theta_{i\text{arm}}$	d	α	l
0	$\theta_{1\text{arm}}$-90^o	0	90 ^{o}	0
1	$\theta_{2\text{arm}}$	0	-90 ^{o}	0
2	$\theta_{3\text{arm}}$	0	0	l_1
3	0	0	0	l_2

Table 2. Link parameters of the robot arm.

Here, variable factor θ_i is the joint angle between the X_{i-1} and the X_i axes measured about the Z_i axis; d_i is the distance from the X_{i-1} axis to the X_i axis measured along the Z_i axis; α_i is the angle between the Z_i axis to the Z_{i-1} axis measured about the X_{i-1} axis, and l_i is the distance from the Z_i axis to the Z_{i-1} axis measured along the X_{i-1} axis. Here, link length for the upper and lower arm is described as l_1 and l_2, respectively. The following Eq. (13) is used to obtain the forward kinematics solution for the robot arm.

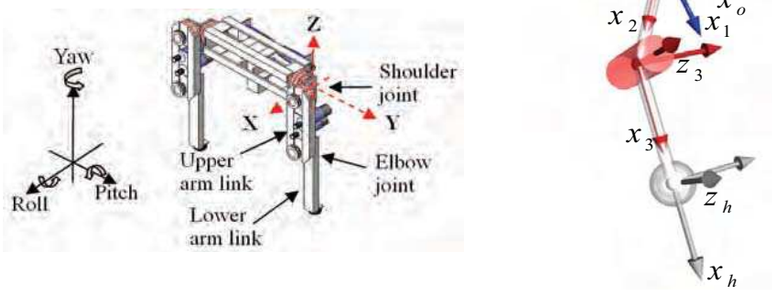

Fig. 12. Arm structure and configurations of joint coordinates at the robot arm of *Bonten-Maru II.*

$$ {}^{o}_{h}T = {}^{0}_{1}T\,{}^{1}_{2}T\,{}^{2}_{3}T\,{}^{3}_{h}T = \begin{bmatrix} s_1c_{23} & -s_1s_{23} & c_1 & s_1(l_1c_2 + l_2c_{23}) \\ s_{23} & c_{23} & 0 & l_1s_2 + l_2s_{23} \\ -c_1c_{23} & c_1s_{23} & s_1 & -c_1(l_1c_2 + l_2c_{23}) \\ 0 & 0 & 0 & 1 \end{bmatrix} \tag{13} $$

The end-effector's orientation with respect to the reference coordinate (${}^{o}_{h}R$) is shown in Eq. (14), while the position of the end effector (${}^{0}P_h$) is shown in Eq. (15). The position of the end effector in regard to global axes P_x, P_y and P_z can be define by Eq. (16). Here, s_i and c_i are respective abbreviations of $\sin\theta_i$ and $\cos\theta_i$, where (i=1,2,…,n) and n is equal to quantity of DOF.

$$ {}^{o}_{h}R_{\text{arm}} = \begin{bmatrix} s_1c_{23} & -s_1s_{23} & c_1 \\ s_{23} & c_{23} & 0 \\ -c_1c_{23} & c_1s_{23} & s_1 \end{bmatrix} \tag{14} $$

$$ {}^{o}P_{h\,\text{arm}} = \begin{bmatrix} s_1(l_1c_2 + l_2c_{23}) \\ l_1s_2 + l_2s_{23} \\ -c_1(l_1c_2 + l_2c_{23}) \end{bmatrix} \tag{15} $$

$$\left.\begin{aligned} P_{x\,\mathrm{arm}} &= s_1(l_1c_2 + l_2c_{23}) \\ P_{y\,\mathrm{arm}} &= l_1s_2 + l_2s_{23} \\ P_{z\,\mathrm{arm}} &= -c_1(l_1c_2 + l_2c_{23}) \end{aligned}\right\} \tag{16}$$

As understood from Eqs. (14) and (15), a forward kinematics equation can be used to compute the Cartesian coordinates of the robot arm when the joint angles are known. However, in real-time applications it is more practical to provide the end effector's position and orientation data to the robot's control system than to define each joint angle that involved complicated calculations. Therefore, inverse kinematics solutions are more favorable for generating the trajectory of the humanoid robot manipulator. To define joint angles $\theta_{1\mathrm{arm}}$, $\theta_{2\mathrm{arm}}$, $\theta_{3\mathrm{arm}}$ in an inverse kinematics problem, at first each position element in Eq. (16) is multiplied and added to each other according to Eq. (17), which can also be arranged as Eq. (18). Thus, $\theta_{3\mathrm{arm}}$ is defined in Eq. (19).

$$P_{x\,\mathrm{arm}}{}^2 + P_{y\,\mathrm{arm}}{}^2 + P_{z\,\mathrm{arm}}{}^2 = l_1{}^2 + l_2{}^2 + 2l_1l_2c_3 \tag{17}$$

$$c_3 = \frac{P_{x\,\mathrm{arm}}{}^2 + P_{y\,\mathrm{arm}}{}^2 + P_{z\,\mathrm{arm}}{}^2 - (l_1{}^2 + l_2{}^2)}{2l_1l_2} = C \tag{18}$$

$$\theta_{3\,\mathrm{arm}} = \mathrm{Atan2}\left(\pm\sqrt{1 - C^2}, C\right) \tag{19}$$

Referring to the rotation direction of $\theta_{3\mathrm{arm}}$, if $sin\theta_{3\mathrm{arm}}$ is a positive value, it describes the inverse kinematics for the right arm, while if it is a negative value it described the left arm. Consequently, $\theta_{3\mathrm{arm}}$ is used to define $\theta_{2\mathrm{arm}}$, as shown in Eqs. (20) ~ (22), where newly polar coordinates are defined in Eq. (22). Finally, by applying formulation in Eqs. (23) and (24), $\theta_{1\mathrm{arm}}$ can be defined as in Eq. (25).

$$k_1 = l_1 + l_2c_3, \qquad k_2 = -l_2s_3 \tag{20}$$

$$p_{xz} = k_1c_2 + k_2s_2, \qquad p_y = k_2c_2 - k_1s_2 \tag{21}$$

$$\phi = \mathrm{Atan2}\ (k_1, k_2) \tag{22}$$

$$\phi + \theta_{2\,\mathrm{arm}} = \mathrm{Atan2}\left(\frac{p_{xz}}{r}, \frac{p_y}{r}\right) = \mathrm{Atan2}\ (p_{xz}, p_y) \tag{23}$$

$$\theta_{2\,\mathrm{arm}} = \mathrm{Atan2}\ (p_{xz}, p_y) - \mathrm{Atan2}\ (k_1, k_2) \tag{24}$$

$$\theta_{1\,\mathrm{arm}} = \mathrm{Atan2}\left(\frac{p_x}{p_{xz}}, \frac{p_z}{p_{xz}}\right) = \mathrm{Atan2}\ (p_x, p_z) \tag{25}$$

6.2 Kinematics analysis of a 6-DOF humanoid robot's leg

Each of the legs has six DOFs: three DOFs (yaw, roll and pitch) at the hip joint, one DOF (pitch) at the knee joint and two DOFs (pitch and roll) at the ankle joint. In this research, we solve only inverse kinematics calculations for the robot leg. A reference coordinate is taken at the intersection point of the three-DOF hip joint. In solving calculations of inverse

kinematics for the leg, just as for arm, the joint coordinates are divided into eight separate coordinate frames as listed bellow.

Σ_0 : Reference coordinate.

Σ_1 : Hip yaw coordinate.

Σ_2 : Hip roll coordinate.

Σ_3 : Hip pitch coordinate.

Σ_4 : Knee pitch coordinate.

Σ_5 : Ankle pitch coordinate.

Σ_6 : Ankle roll coordinate.

Σ_h : Foot bottom-center coordinate.

Figure 13 shows the structure and distribution of joints and links in the robot's leg. This figure also shows a model of the robot leg that indicates the distributions and orientation of each set of joint coordinates. Here, link length for the thigh is l_1, while for the shin it is l_2. The same convention applies for the arm link parameter mentioned earlier. Link parameters for the leg are defined in Table 3. Referring to Fig. 13, the transformation matrix at the bottom of the foot (^6_hT) is an independent link parameter because the coordinate direction is changeable. Here, to simplify the calculations, the ankle joint is positioned so that the bottom of the foot settles on the floor surface. The leg's orientation is fixed from the reference coordinate so that the third row of the rotation matrix at the leg's end becomes like following:

$$P_z \text{leg} = [0 \quad 0 \quad 1]^T \tag{26}$$

Furthermore, the leg's links are classified into three groups to short-cut the calculations, where each group of links is calculated separately as follows.

i) From link 0 to link 1 (Reference coordinate to coordinate joint number 1).
ii) From link 1 to link 4 (Coordinate joint number 2 to coordinate joint number 4).
iii) From link 4 to link 6 (Coordinate joint number 5 to coordinate at the foot bottom).

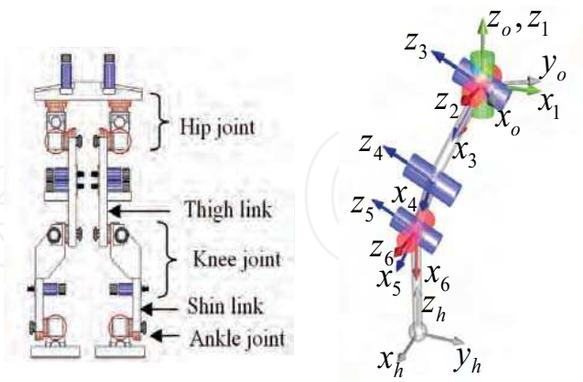

Fig. 13. Structure and configurations of joint coordinates at the robot leg of *Bonten-Maru II*.

Link	$\theta_{i\text{leg}}$	*d*	α	*l*
0	$\theta_{1\text{leg}}+90^{o}$	*0*	*0*	*0*
1	$\theta_{2\text{leg}}-90^{o}$	*0*	*90*	*0*
2	$\theta_{3\text{leg}}$	*0*	*90*	*0*
3	$\theta_{4\text{leg}}$	*0*	*0*	l_1
4	$\theta_{5\text{leg}}$	*0*	*0*	l_2
5	$\theta_{6\text{leg}}$	*0*	*-90*	*0*
6	*0*	*0*	*0*	l_3

Table 3. Link parameters of the leg.

Basically, i) is to control leg rotation at the *Z*-axis, ii) is to define the leg position, while iii) is to decide the leg's end-point orientation. A coordinate transformation matrix can be arranged as below.

$$ {}^{o}_{h}T = {}^{o}_{1}T\,{}^{1}_{4}T\,{}^{4}_{h}T = ({}^{o}_{1}T)({}^{1}_{2}T\,{}^{2}_{3}T\,{}^{3}_{4}T)({}^{4}_{5}T\,{}^{5}_{6}T\,{}^{6}_{h}T) \tag{27} $$

Here, the coordinate transformation matrices for ${}^{1}_{4}T$ and ${}^{4}_{h}T$ can be defined as Eqs. (28) and (29), respectively.

$$ {}^{1}_{4}T = {}^{1}_{2}T\,{}^{2}_{3}T\,{}^{3}_{4}T = \begin{bmatrix} s_2c_{34} & -s_2s_{34} & -c_2 & l_1s_2c_3 \\ -s_{34} & -c_{34} & 0 & -l_1s_3 \\ -c_2c_{34} & c_2s_{34} & -s_2 & -l_1c_2c_3 \\ 0 & 0 & 0 & 1 \end{bmatrix} \tag{28} $$

$$ {}^{4}_{h}T = {}^{4}_{5}T\,{}^{5}_{6}T\,{}^{6}_{h}T = \begin{bmatrix} c_5c_6 & -c_5s_6 & -s_5 & l_2 + l_3c_5c_6 \\ s_5c_6 & -s_5s_6 & c_5 & l_3s_5c_6 \\ -s_6 & -c_6 & 0 & -l_3s_6 \\ 0 & 0 & 0 & 1 \end{bmatrix} \tag{29} $$

The coordinate transformation matrix for ${}^{0}_{h}T$, which describes the leg's end-point position and orientation, can be shown with the following equation.

$$ {}^{o}_{h}T = \begin{bmatrix} r_{11} & r_{12} & r_{13} & p_x \\ r_{21} & r_{22} & r_{23} & p_y \\ r_{31} & r_{32} & r_{33} & p_z \\ 0 & 0 & 0 & 1 \end{bmatrix} \tag{30} $$

From Eq. (26), the following conditions were satisfied.

$$ r_{13} = r_{23} = r_{31} = r_{32} = 0 \quad , \quad r_{33} = 1 \tag{31} $$

Hence, joint rotation angles $\theta_{1\text{leg}}$~$\theta_{6\text{leg}}$ can be defined by applying the above conditions.
First, considering i), in order to provide rotation at the *Z*-axis, only the hip joint needs to rotate in the yaw direction, specifically by defining $\theta_{1\text{leg}}$. As mentioned earlier, the bottom of the foot settles on the floor surface; therefore, the rotation matrix for the leg's end-point measured from the reference coordinate can be defined by the following Eq. (32). Here, $\theta_{1\text{leg}}$ can be defined as below Eq. (33).

$$ {}^{o}_{h}R = \mathrm{Rot}(z,\theta_{1\mathrm{leg}}) = \begin{bmatrix} c\theta_{1\mathrm{leg}} & -s\theta_{1\mathrm{leg}} & 0 \\ s\theta_{1\mathrm{leg}} & c\theta_{1\mathrm{leg}} & 0 \\ 0 & 0 & 1 \end{bmatrix} = \begin{bmatrix} r_{11} & r_{12} & 0 \\ r_{21} & r_{22} & 0 \\ 0 & 0 & 1 \end{bmatrix} \tag{32} $$

$$ \theta_{1\mathrm{leg}} = \mathrm{Atan2}\left(r_{21}, r_{22}\right) \tag{33} $$

Next, considering ii), from the obtained result of $\theta_{1\mathrm{leg}}$, ${}^{o}_{h}T$ is defined in following equation:

$$ {}^{o}_{h}T = \begin{bmatrix} -s_1 & -c_1 & 0 & P_{x\,\mathrm{leg}} \\ c_1 & -s_1 & 0 & P_{y\,\mathrm{leg}} \\ 0 & 0 & 1 & P_{z\,\mathrm{leg}} \\ 0 & 0 & 0 & 1 \end{bmatrix} \tag{34} $$

Here, from constrain orientation of the leg's end point, the position vector of joint 5 is defined as follows in Eq. (35), and its relative connection with the matrix is defined in Eq. (36). Next, equation (37) is defined relatively.

$$ {}^{o}P_5 = {}^{o}_{4}T\,{}^{4}P_5 = \begin{bmatrix} P_{x\,\mathrm{leg}} & P_{y\,\mathrm{leg}} & P_{z\,\mathrm{leg}} - l_3 \end{bmatrix}^T \tag{35} $$

$$ {}^{1}_{4}T\,{}^{4}\hat{P}_5 = {}^{o}_{1}T^{-1}\,{}^{o}\hat{P}_5 \tag{36} $$

$$ \begin{bmatrix} s_2c_{34} & -s_2s_{34} & -c_2 & l_1s_2c_3 \\ -s_{34} & -c_{34} & 0 & -l_1s_3 \\ -c_2c_{34} & c_2s_{34} & -s_2 & -l_1c_2c_3 \\ 0 & 0 & 0 & 1 \end{bmatrix} \begin{bmatrix} l_2 \\ 0 \\ 0 \\ 1 \end{bmatrix} = \begin{bmatrix} -s_1 & c_1 & 0 & 0 \\ -c_1 & -s_1 & 0 & 0 \\ 0 & 0 & 1 & 0 \\ 0 & 0 & 0 & 1 \end{bmatrix} \begin{bmatrix} p_x \\ p_y \\ p_z - l_3 \\ 1 \end{bmatrix} \tag{37} $$

Therefore,

$$ \begin{bmatrix} \hat{P}_{x\,\mathrm{leg}} \\ \hat{P}_{y\,\mathrm{leg}} \\ \hat{P}_{z\,\mathrm{leg}} \end{bmatrix} = \begin{bmatrix} s_2\left(l_1c_3 + l_2c_{34}\right) \\ -\left(l_1c_3 + l_2s_{34}\right) \\ -c_2\left(l_1c_3 + l_2c_{34}\right) \end{bmatrix} \tag{38} $$

To define joint angles $\theta_{2\mathrm{leg}}$, $\theta_{3\mathrm{leg}}$, $\theta_{4\mathrm{leg}}$, Eq. (38) is used, and it is similar to the calculation for solving inverse kinematics using Eq. (16) for the arm. Therefore, the rotation angles are defined as the following equations.

$$ \theta_{4\,\mathrm{leg}} = \mathrm{Atan2}\left(\pm\sqrt{1 - C^2}, C\right) \tag{39} $$

$$ \theta_{3\mathrm{leg}} = \mathrm{Atan2}\left(\hat{p}_{xz\,\mathrm{leg}}, \hat{p}_{y\,\mathrm{leg}}\right) + \mathrm{Atan2}\left(k_1, k_2\right) \tag{40} $$

$$ \theta_{2\,\mathrm{leg}} = \mathrm{Atan2}\left(\hat{p}_{x\,\mathrm{leg}}, \hat{p}_{z\,\mathrm{leg}}\right) \tag{41} $$

Eventually, $C, \hat{p}_{xz\,\mathrm{leg}}, k_1, k_2$ are defined as follows.

$$C = \frac{\hat{p}_{x\,\mathrm{leg}}{}^2 + \hat{p}_{y\,\mathrm{leg}}{}^2 + \hat{p}_{z\,\mathrm{leg}}{}^2 - (l_1{}^2 + l_2{}^2)}{2l_1 l_2} \tag{42}$$

$$\hat{p}_{xz\,\mathrm{leg}} = \sqrt{\hat{p}_{x\,\mathrm{leg}}{}^2 + \hat{p}_{z\,\mathrm{leg}}{}^2} \tag{43}$$

$$\begin{cases} k_1 = l_1 + l_2 c_4 \\ k_2 = -l_2 s_4 \end{cases} \tag{44}$$

Finally, considering iii), joint angles $\theta_{5\mathrm{leg}}$ and $\theta_{6\,\mathrm{leg}}$ are defined geometrically by the following equations.

$$\theta_{5\,\mathrm{leg}} = -\theta_{3\,\mathrm{leg}} - \theta_{4\,\mathrm{leg}} \tag{45}$$

$$\theta_{6\,\mathrm{leg}} = -\theta_{2\,\mathrm{leg}} \tag{46}$$

6.3 Interpolation of Manipulator's End-Effector

A common way of making a robot's manipulator to move from start point P_0 to finish point P_f in a smooth, controlled fashion is to have each joint to move as specified by a smooth function of time. Each joint starts and ends its motion at the same time, thus the robot's motion appears to be coordinated. To compute these motions, in the case that start position P_0 and end position P_f are given, interpolation of time t using polynomial equations is performed to generate trajectory. In this research, we employ degree-5 polynomial equations as shown in Eq. (47) to solve interpolation from P_0 to P_f. Time factors at P_0 and P_f are expressed as t_0=0 and t_f, respectively.

$$P(t) = a_0 + a_1 t + a_2 t^2 + a_3 t^3 + a_4 t^4 + a_5 t^5 \tag{47}$$

Here, coefficient a_i (i=0, 1,.., 5) is defined by solving deviations of $P(0), \dot{P}(0), \ddot{P}(0), P(t_f), \dot{P}(t_f), \ddot{P}(t_f)$. In this study, velocity and acceleration at P_0 and P_f are defined as zero; only the position factor is considered as a coefficient for performing interpolation. Finally the interpolation equation is defined by Eq. (48), where $u = \frac{t}{t_f} = \frac{current\ \ time}{motion\ \ time}$.

$$P(t) = P_0 + 10\left(P_f - P_0\right)u^3 - 15\left(P_f - P_0\right)u^4 + 6\left(P_f - P_0\right)u^5 \tag{48}$$

7. Experimental Results and Discussion

7.1 Experimental Procedure

Experiments were conducted in conjunction with the groping locomotion experiments. Initially, a series of motion programs were created and saved in the robot's control system. Before performing the experiments, a simulation using animation that applies GNUPLOT was performed for analysis and confirmation of the robot joint's trajectory generation. Figure 14 presents the animation screen of the robot's trajectory, which features a robot control process and motion instructor process. This figure also shows the path planning of humanoid robot navigation performed in the experimet. Each joint's rotation angles are saved and analyzed in a graph structure. This is to ensure the computation of joints rotation

angle was correct and according to result of groping locomotion. For example, graphs for the left and right leg are plotted in Fig. 15 and Fig. 16 respectively during obstacle avoidance. The graphs show the smooth trajectory of the rotation angles at each leg's joint. In this experiment, the wall is positioned at the robot's front and its right side, while an obstacle is on its left side. The obstacle height is about same with the robot shoulder. During experiments, at first the robot performing groping locomotion to define groping angle, then continuously performs the obstacle avoidance. The experiment is conducted in autonomous way and the performance is evaluated by observation. In order to recognize objects, six-axis force sensors were attached to the robot arms. The utilized force sensors are designed to detect three force components in each axial direction, with the other three components of moment around each axis operating simultaneously and continuously in real time with high accuracy. The maximum loads at the *XY*-axes are 400 N, while at the *Z*-axis it is 200 N.

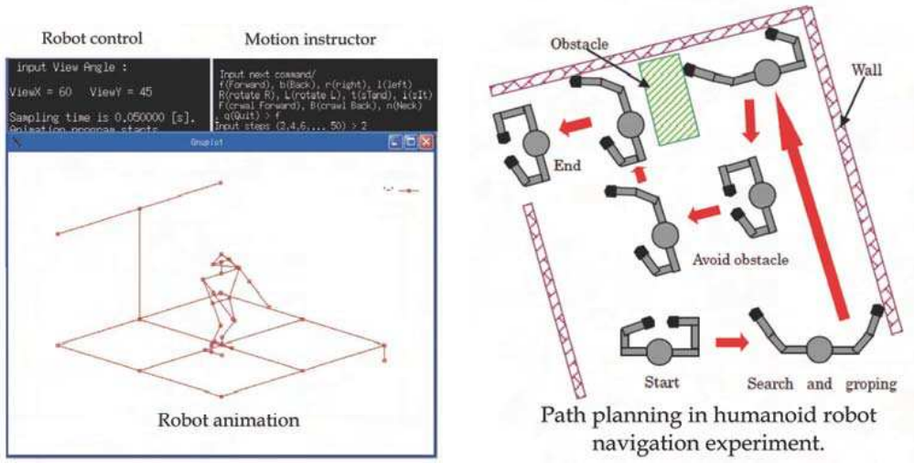

Fig. 14. Animation of the robot's trajectory and path planning of the experiment

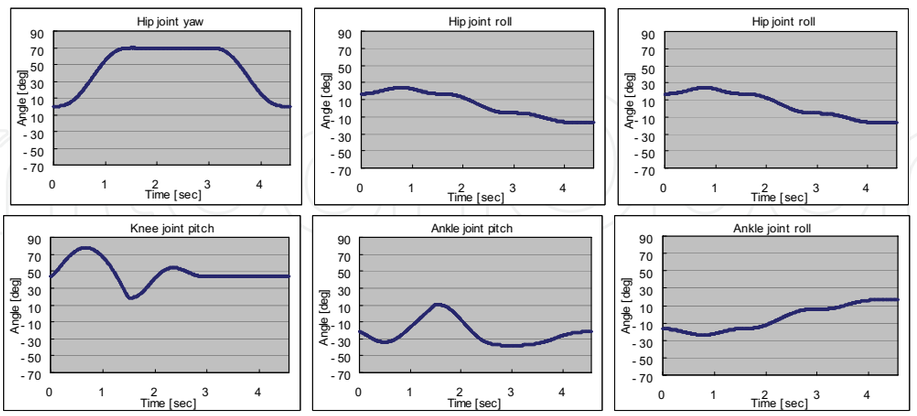

Fig. 15. Rotation angle of the left leg joints in the obstacle avoidance.

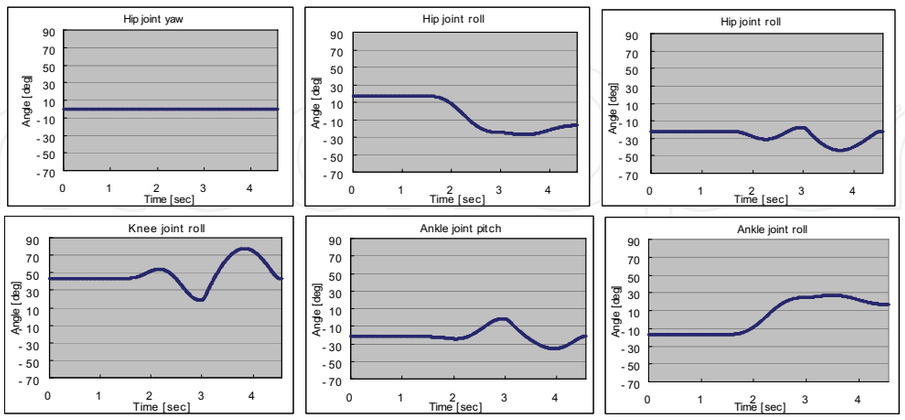

Fig. 16. Rotation angle of the right leg joints in the obstacle avoidance.

7.2 Results of Humanoid Robot Locomotion

Figure 17 shows sequential photographs of the actual robot's locomotion during experiments on groping front wall, Meanwhile Fig. 18 shows sequential photographs of groping right-side wall experiment. Consiquently, the humanoid robot performed the obstacle avoidance as shown in Fig. 19. The experimental results reveal that the robot's arm and legs move in a smooth and controlled motion to perform tasks in groping locomotion and obstacle avoidance. The formulations from the proposed groping locomotion algorithm guided the robot locomotion to recognize wall's orientation and correct robot's distance and angle based on the groping result. Meanwhile formulations in obstacle avoidance algorithm combined with groping locomotion algorithm recognize the presence of obstacle and perform suitable trajectory to avoid the obstacle. The proposed kinematics and interpolation formulation generate smooth trajectory for the arms and legs during performing locomotion in groping locomotion and obstacle avoidance experiments.

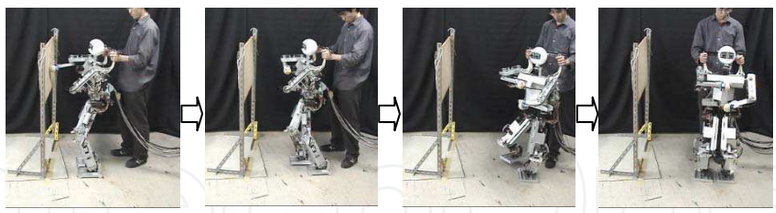

Fig. 17. Sequential photograph of groping front wall experiment.

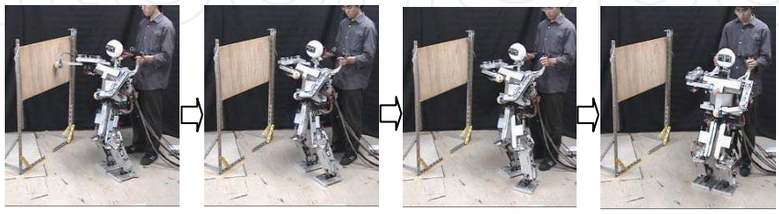

Fig. 18. Sequential photograph of groping right-side wall experiment.

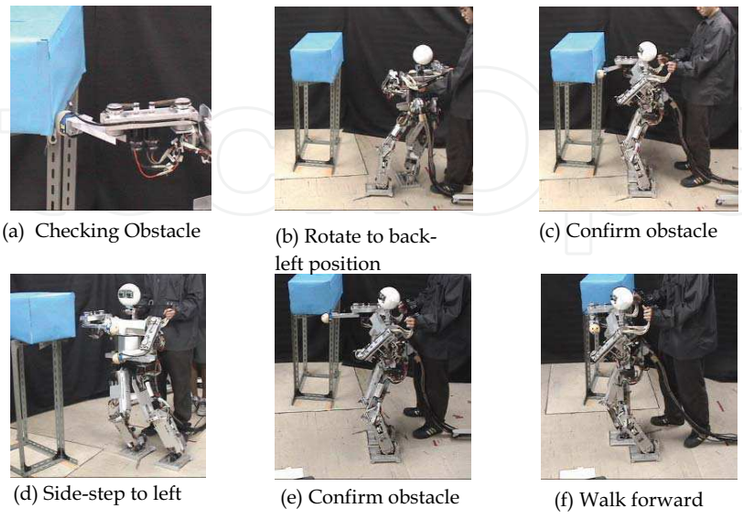

Fig. 19. Sequential photograph of obstacle avoidance in groping locomotion experiment.

8. Conclusion

The development of autonomous navigation system for humanoid robot to solve the problem of "working coexistence" of humans and robots is an important issue. It is apparent that the common living and working environment to be shared by humanoid robots is presently adapted mainly to human, and it cannot be expected that this will be significantly changed to suit the needs of robots. Hence, the problem of human-humanoid robot interaction, and humanoid robot-surrounding environment interaction are become the research topics that are gaining more and more in importance. Furthermore, contact interaction-based navigation system is practically significant for humanoid robots to accurately structure and recognize their surrounding conditions (Ellery, 2005, Salter et al., 2006).

Research on groping locomotion in humanoid robot's navigation system has led to the proposal of a basic contact interaction method for humanoid robots to recognize and respond to their surrounding conditions. This research proposed a new obstacle avoidance method which applied reliable algorithms in a humanoid robot control system in conjunction with the groping-locomotion algorithm. The proposed method is based on contact interaction whereby the robot arms directly touch and analyze an object, with the aim of accomplishing the objective of developing an interaction method for the humanoid robot and its surroundings. Performance of the proposed method was evaluated by experiments using prototype humanoid robot *Bonten-Maru II* which force sensors are attached to its arms as end-effector to detect and recognize objects.

The experimental results indicated that the humanoid robot could recognize the existence of an obstacle and could avoid it by generating suitable leg trajectories. The proposed algorithm was effectively operated in conjunction with the groping locomotion algorithm to detect and avoid obstacle in the correction area, which improved the performance of the groping locomotion. Regarding the motion of the

humanoid robot's arms, the proposed algorithm provides a good relationship between groping locomotion and obstacle avoidance. It demonstrates intelligent detection of most objects around the robot, enabling the robot's control system to effectively identify the object position and perform necessary locomotion.
In the experiments with humanoid robot, autonomous motions of the robot's manipulators are managed to demonstrate. These satisfy the objective of this research to develop an autonomous navigation system for bipedal humanoid robot to recognize and avoid obstacles in groping locomotion. Consiquently, the proposed groping locomotion method clearly demonstrated two important tasks to solve in the autonomous navigation for walking robots: self-localization and obstacle avoidance.
The proposed idea should contribute to better understanding of interactions between a robot and its surroundings in humanoid robot's navigation. Furthermore, future refinement of the proposed idea in various aspects will result in better reliability of the groping locomotion mechanism, enabling any type of anthropomorphic robots fitted with it to operate effectively in the real environments. It is anticipated that using this novel humanoid robot's navigation system technology will bring forward the evolution of human and humanoid robots working together in real life.

9. Future Development: Development of Object Handling

As mentioned in previous section, an autonomous navigation in walking robots requires that three main tasks be solved: self-localization, obstacle avoidance, and object handling. In current research, we proposed a basic humanoid robot navigation system called the "groping locomotion" for a 21-DOF humanoid robot, which is capable of defining self-localization and obstacle avoidance.
In future work, we going to focus on development of the object handling. Although current robot hands are equipped with force sensors to detect contact force, they do not make use of sensors capable of detecting an object's hardness and/or softness, nor can they recognize the shape that they grip. For a robot hand to grip an object without causing damage to it, or otherwise damaging the sensor itself, it is important to employ sensors that can adjust the gripping power. Recently, with the aim to determining physical properties and events through contact during object handling, we are in progress of developing a novel optical three-axis tactile sensor capable of acquiring normal and shearing force (Ohka et al., 2006). A tactile sensor system is essential as a sensory device to support the robot control system (Lee & Nicholls, 1999, Kerpa et al., 2003). This tactile sensor is capable of sensing normal force, shearing force, and slippage, thus offering exciting possibilities for application in the field of robotics for determining object shape, texture, hardness, etc. The tactile sensor system developed in this research is combined with 3-DOF humanoid robot finger system where the tactile sensor in mounted on the fingertip.
Future work will involve further development of the contact-based humanoid robot navigation system project, applying the integrated system comprising the optical three-axis tactile sensor and robot fingers in humanoid robot's control system for object handling purposes.

10. Acknowledgements

This research project is partly supported by fiscal 2006 grants from the Ministry of Education, Culture, Sports, Science and Technology (the Japan Scientific Research of

Priority Areas 438 "Next-Generation Actuators Leading Breakthroughs" program, No. 16078207).

11. References

Ellery, A. (2005). Environment-robot interaction-the basis for mobility in planetary micro-rovers, *Journal Robotics and Autonomous Systems,* Vol. 51, pp. 29-39

Borenstein, J. & Koren, Y. (1991). Histogramic in-motion mapping for mobile robot obstacle avoidance, *Journal of Robotics and Automation*, Vol. 7, No. 4, pp. 535-539

Cheng, G.; Nagakubo, A. & Kuniyoshi, Y. (2001). Continuous Humanoid Interaction: An Integrated Perspective -Gaining Adaptivity, Redundancy, Flexibility- in One, *Journal of Robotics and Autonomous Systems*, Vol. 37, Issues 2-3 pp 161-183

Coelho, J.; Piater, J. & Grupen, R. (2001). Developing Haptic and Visual Perceptual Categories for Reaching and Grasping with a Humanoid Robot, *Journal Robotics and Autonomous Systems*, Vol. 37 pp. 195-218

Clerentin, A.; Delahoche, L.; Brassart, E. & Drocourt, C. (2005). Self localization: a new uncertainty propagation architecture, *Journal of Robotics and Autonomous Systems*, Vol. 51 pp. 151-166

Denavit, J. & Hartenberg, S. (1995). A kinematics notation for lower-pair mechanisms based upon matrices, *Journal of Applied Mechanics*, Vol. 77, pp. 215-221

Hashimoto, S.; Narita, S.; Kasahara, H.; Takanishi, A.; Sugano, S.; Shirai, K.; Kobayashi, T.; Takanobu, H.; Kurata, T.; Fujiwara, K.; Matsuno, T.; Kawasaki, T. & Hoashi, K. (1997). Humanoid Robot-Development of an Information Assistant Robot Hadaly, *Proceeding 6th IEEE Int. Workshop Robot and Human Communication (ROMAN'97)*, pp. 106-111

Hirai, K.; Hirose, M.; Haikawa, Y. & Takenaka, T. (1998). The development of Honda humanoid robot, *Proceedings of International Conference on Robotics and Automation'98*, pp. 1321-1326

Hirukawa, H.; Kanehiro, F & Kaneko, K. (2004). Humanoid robotics platforms developed in HRP, *Journal of Robotics and Automation Systems*, Vol. 48, pp. 165-175

Hanafiah, Y.; Yamano, M.; Nasu, Y. & Ohka, M. (2005a). Obstacle avoidance in groping locomotion of a humanoid robot, *Journal of Advanced Robotic Systems*, Vol.2, No. 3, pp. 251-258, ISSN 1729-5506

Hanafiah, Y.; Yamano, M.; Nasu, Y. & Ohka, M., (2005b). Analysis of correction of humanoid robot locomotion direction in groping locomotion method, *Proceeding International Advance Technology Congress 2005 (ATCI'05)*, CISAR-15, CD-ROM, ISBN 983-42758-1-1

Hanafiah, Y.; Yamano, M.; Nasu, Y. & Ohka, M. (2005c). Trajectory generation in groping locomotion of a 21-DOF humanoid robot, *Proceedings 9th International Conference on Mechatronics Technology 2005 (ICMT'05)*, CD-ROM

Konno, A. (1999). Development of an Anthropomorphic Multi-Finger Hand and Experiment on Grasping Unknown Object by Groping, *Transaction of the JSME*, Vol.65, No. 638, pp 4070-4075

Kanda, T.; Ishiguro, H.; Ono, Y.; Imai, M. & Nakatsu, R. (2002). Development and Evaluation of an Interactive Humanoid Robot Robovie, *Proceeding IEEE Int. Conf. Robotics and Automation (ICRA'02)*, Vol. 2, pp. 1848-1855

Kaneko, K.; Kanehiro, F.; Kajita, S.; Yokoyama, K.; Akachi, K.; Kawasaki, T.; Ota, S. & Isozumi, T. (2002). Design of Prototype Humanoid Robotics Platform for HRP, *Proceeding of the 2002 IEEE/RSJ Intl. Conference on Intelligent Robots and Systems*, pp. 2431-2436, EPFL, Lausanne, Switzerland, October 2002

Kerpa, O.; Weiss, K. & Worn, H. (2003). Development of a flexible tactile sensor system for a humanoid robot, *Proceedings Intl. Conf. on Intelligent Robots and Systems IROS2003*, CD-ROM

Kim, J.; Park, J.; Hwang, Y.K. & Lee, M. (2004). Advance grasp planning for handover operation between human and robot: three handover methods in esteem etiquettes using dual arms and hands of home-service robot, *Proceeding 2nd Int. Conf. on Autonomous Robots and Agents (ICARA'04)*, pp. 34-39

Kajita, S.; Nagasaki, T.; Kaneko, K.; Yokoi, K. & Tanie, K. (2005). A running controller of humanoid biped HRP-2LR, *Proceeding of International Conference on Robotics and Automation '05*, pp. 618-624

Koker, R. (2005). Reliability-based approach to the inverse kinematics solution of robots using Elman's network, *Journal of Engineering Application of Artificial Intelligence*, Vol. 18, No. 6, pp. 685-693

Lee, M.H. & Nicholls, H.R. (1999). Tactile sensing for mechatronics – a state of the art survey, *Journal Mechatronics*, vol. 9, pp. 1-31

Ogata, T.; Matsuyama, Y.; Komiya, T.; Ida, M.; Noda, K. & Sugano, S. (2000). Development of Emotional Communication Robot: WAMOEBA-2R-Experimental Evaluation of the Emotional Communication between Robots and Human, *Proceeding of IEEE /RSJ Intelligent Robots and Systems (IROS-00)*, Vol. 1, pp. 175-180

Osswald, D.; Martin, J.; Burghart, C.; Mikut, R.; Worn, H. & Bretthauer, G., (2004). Integrating a Flexible Anthropomorphic, Robot Hand into the Control, System of a Humanoid Robot, *Journal of Robotics and Autonomous Systems*, Vol. 48, Issue 4, pp. 213-221

Omata, S.; Murayama, Y. & Constantinou, C.E. (2004). Real time robotic tactile sensor system for determination of the physical properties of biomaterials, *Journal of Sensors and Actuators A*, Vol. 112, pp. 278-285

Ohka, M.; Kobayashi, H. & Mitsuya, Y. (2006). Sensing precision of an optical three-axis tactile sensor for a robotic finger, *Proceeding 15th IEEE International Symposium on Robot and Human Interactive Communication (RO-MAN2006*)

Sian, N.E.; Yokoi, K.; Kajita, S.; Kanehiro, F. & Tanie, K. (2002). Whole body teleoperation of a humanoid robot –development of a simple master device using joysticks-, *Proc. Of the 2002 IEEE/RSJ Intl. Conf. on Intelligent Robots and Systems EPFL*, pp. 2569-2574, Lausanne, Switzerland, October 2002

Seydou, S.; Ohya, A. &Yuta, S. (2002). Real-time obstacle avoidance by an autonomous mobile robot using an active vision sensor and a vertically emitted laser slit, *Proceeding of the 7th International Conference on Intelligent Autonomous Systems*, California, USA, pp. 301-308, March 2002

Seara, J.F. & Schmidt, G. (2004). Intelligent gaze control for vision-guided humanoid walking: methodological aspects, *Journal of Robotics and Autonomous System*, Vol. 48, pp. 231-248

Salter, T.; Dautenhahn, K. & Boekhorst R. (2006). Learning About Natural Human-Robot Interaction Styles, *Journal of Robotics and Autonomous Systems*, Vol.52, Issue 2, pp.127-134

Tu, K.Y. & Baltes, J. (2006). Fuzzy potential energy for a map approach to robot navigation, *Journal of Robotics and Autonomous Systems,* Vol. 54, Issue 7, pp. 574-58931, July 2006

Vukobratovic, M.; Borovac, B. & Babkovic, K. (2005). Contribution to the study of Anthropomorphism of Humanoid Robots, *Journal Humanoids Robotics*, Vol. 2, No. 3, pp. 361-387

Mobile Robots: towards New Applications

Edited by Aleksandar Lazinica

ISBN 978-3-86611-314-5

Hard cover, 600 pages

Publisher I-Tech Education and Publishing

Published online 01, December, 2006

Published in print edition December, 2006

The range of potential applications for mobile robots is enormous. It includes agricultural robotics applications, routine material transport in factories, warehouses, office buildings and hospitals, indoor and outdoor security patrols, inventory verification, hazardous material handling, hazardous site cleanup, underwater applications, and numerous military applications. This book is the result of inspirations and contributions from many researchers worldwide. It presents a collection of wide range research results of robotics scientific community. Various aspects of current research in new robotics research areas and disciplines are explored and discussed. It is divided in three main parts covering different research areas: Humanoid Robots, Human-Robot Interaction, and Special Applications. We hope that you will find a lot of useful information in this book, which will help you in performing your research or fire your interests to start performing research in some of the cutting edge research fields mentioned in the book.

InTech Europe

University Campus STeP Ri
Slavka Krautzeka 83/A
51000 Rijeka, Croatia
Phone: +385 (51) 770 447
Fax: +385 (51) 686 166
www.intechopen.com

InTech China

Unit 405, Office Block, Hotel Equatorial Shanghai
No.65, Yan An Road (West), Shanghai, 200040, China
中国上海市延安西路65号上海国际贵都大饭店办公楼405单元
Phone: +86-21-62489820
Fax: +86-21-62489821

IntechOpen